Microplastic particles contain ice nucleation sites that can be deactivated by atmospheric aging

Preprint

Teresa M. Seifried[1], Sepehr Nikkho[1], Aurelio Morales Murillo[2], Lucas J. Andrew[1], Edward R. Grant[1], Allan K. Bertram[1]*

[1] Department of Chemistry, University of British Columbia, Vancouver, British Columbia, V6T 1Z1, Canada;

[2] Faculty of Pharmaceutical Sciences, University of British Columbia, Vancouver, British Columbia, V6T 1Z3, Canada;

* bertram@chem.ubc.ca

KEYWORDS: Microplastics, Ice Nucleation, Ozone, Atmospheric Oxidation

SYNOPSIS: Minimal research exists on microplastics impact on atmospheric ice nucleation. This study reports on the ability for microplastics to nucleate ice heterogeneously and how atmospheric aging influences this ability with implications to cloud glaciation.

Abstract

Recent research has shown that microplastics are widespread in the atmosphere. However, we know little about their ability to nucleate ice and impact cloud glaciation. Ice nucleation by microplastics could also limit their long-range transport and global distributions. The present study explores the heterogeneous ice nucleation activity of seven microplastic samples in the immersion-freezing mode. Two polypropylene and one polyethylene terephthalate sample froze heterogeneously with median freezing temperatures of -20.9°C, -23.2°C and -21.9°C, respectively. The number of ice nucleation sites per surface area, $n_s(T)$, ranged from 10^{-1} to 10^4 cm^{-2} in a temperature interval of -15 to -25°C, which is comparable to that of volcanic ash and fungal spores. After exposure to ozone or a combination of UV light and ozone, simulating atmospheric aging, the ice nucleation activity decreased in some cases and remained unchanged in others. An initial assessment using microplastic concentrations reported in the literature and our freezing data suggest that microplastics may influence cloud glaciation in some situations, but more studies are needed to confirm this initial assessment. Ice nucleation by microplastics may also impact their long-range transport and global distribution of microplastics based on a comparison of our freezing results and those of fungal spores.

Introduction

In the absence of ice-nucleating particles (INPs) in the atmosphere, cloud droplets freeze homogeneously at a temperature of approximately -35°C.[1,2] In the presence of INPs, cloud droplets can freeze at higher temperatures. After INPs initiate the formation of ice in cloud droplets, the resulting ice crystals can grow by the Wegener-Bergeron-Findeisen process and collisions.[3] Notably, a substantial fraction of global precipitation proceeds via these processes.[4,5] INPs also influence the optical properties and lifetimes of clouds, with implications for the albedo effect. Atmospheric ice nucleation thus influences the hydrological cycle and radiative budget, underlining the importance of gaining a comprehensive understanding of the properties, concentration, and sources of INPs in the atmosphere.

The ability of atmospheric particles to nucleate ice also influences their long-range transport and concentrations in the atmosphere. When an aerosol particle triggers ice nucleation followed by precipitation, the atmospheric concentration and long-range transport of the aerosol particles can be reduced. For example, a study by Haga et al.[6] showed that ice nucleation on fungal spores, which have only modest freezing efficiencies, leads to a decrease in the annual mean concentrations of fungal spores in remote regions and the upper troposphere.

Natural sources of INPs include mineral dust[7,8], volcanic ash[9–11], and biological particles (e.g. pollen[12,13], fungal spores[14] and archaea[15]). Possible anthropogenic sources of INPs include soot[16] and coal fly ash.[17,18] With the advent of large-scale plastic production and consumption, microplastics have emerged as a potential new class of anthropogenic INPs.[19,20]

In 2015 Dris et al.[21] first detected microplastic aerosols in the atmosphere. Since then, researchers have tried to identify the sources of these aerosols.[22,23] Tire wear particles from roads are thought to be one of the most significant source of plastics to the atmosphere, followed by

microplastics ejected to the atmosphere with sea spray aerosol and agricultural soil dust.[24] Additionally, microplastics originating from the breakdown of frequently used commercial products, such as polyester clothing, can contribute to the release of plastic fibers into the atmosphere.[25]

Recent studies showed the pivotal role of the atmosphere as a transport system for microplastics connecting natural and urban systems.[27,28] As microplastics get transported throughout the atmosphere, aging is induced by exposure to ultraviolet (UV) radiation and oxidants, such as ozone (O_3). This aging process can oxidize the surface and bulk of microplastics, changing the hydrophobicity/hydrophilicity and chemical properties of the particles. Such changes will likely modify the ability of microplastics to nucleate ice.

Only one study has investigated the ice nucleating ability of microplastics.[19] Ganguly and Ariya[19] synthesized three microplastics types (polypropylene, low-density polyethylene, and high-density polyethylene) in the laboratory and quantified their freezing properties using a droplet freezing technique. This work examined the effect of acidity on freezing, both in pure H_2O and synthetic seawater. In the natural environment, microplastics vary widely in terms of particle composition and morphology. These factors may well affect their ice nucleating capacity, which calls for a wider systematic investigation than has been carried out so far. Studies on the ice nucleation ability of microplastics formed by the breakdown of frequently used products are also necessary as these materials may contribute significantly to the microplastic burden of the atmosphere. Furthermore, the effect of atmospheric aging by O_3 or UV radiation on the ice nucleation properties of microplastics remains unstudied.

Here, we investigate the ice nucleation ability of seven different microplastics substances in the immersion freezing mode. We focus on polymers prevalent in the atmosphere[22]: polypropylene

(PP), polyethylene terephthalate (PET) and polyethylene (PE). For each polymer type, we included at least one commercial sample and one sample generated from the breakdown of a frequently used commercial product. We further test if ice nucleation changes after exposure to O_3 and a combination of UV light and O_3.

Materials and Methods

Samples

Table 1 provides an overview of all samples used. We procured the commercial samples PP-needles[c], PET-spheres[c], and PE-spheres[c] from Nanochemazone (Leduc, AB, Canada) and PP-spheres[c] from Goonvean Fibers (Cullompton, UK). In addition to commercially sourced samples, we generated samples by the breakdown of each polymer type in the laboratory: PP-fibers[b] originating from a PP rope (The Home Depot, Everbilt Light-Duty Diamond Braid Rope, Model # 301831), PE-flakes[b] from a PE cup (The Home Depot, LESSO Test Cap 3, Model # RLN132-030), and PET-fibers[b] originating from PE textile. To obtain PP-fibers[b] and PE-flakes[b], we first cut the rope and the cup into small pieces (approximately 1 cm long), then dipped them into liquid nitrogen, broke them apart using a mortar and pestle, and then passed the material through a filter sieve. PET-fibers[b] were made by Cotton Incorporated (North Carolina, USA), which produces standard fiber textiles for environmental assessments and toxicity studies. We cut the PET fabric into small pieces of approximately 1 cm^2 and then ground them using a Wiley Mill 134.

Table 1. Detailed information about the polymer samples. The superscript ^c in the sample-ID indicates samples of commercial origin; ^b denotes samples obtained from the breakdown of larger plastic pieces.

Polymer type	Origin	Shape	Size	Sample-ID
Polypropylene (PP)	Nanochemazone CAS: 9003-07-0	needles	$d < 30$ μm $l < 150$ μm	*PP-needles[c]*
	Goonvean fibers HM20/70P	spherical	$d \approx 60$ μm	*PP-spheres[c]*
	Rope The Home Depot	fibers	$d \approx 35$ μm $l \approx 800$ μm	*PP-fibers[b]*
Polyethylene terephthalate (PET)	Nanochemazone CAS: 25038-59-9	spherical	$d \approx 80$ μm	*PET-spheres[c]*
	Textile Cotton Inc.	fibers	$d \approx 20$ μm $l \approx 300$ μm	*PET-fibers[b]*
Low density polyethylene (PE)	Nanochemazone CAS: 9002-88-4	spherical	$d \approx 55$ μm	*PE-spheres[c]*
	Cup The Home Depot	flakes	$d \approx 250$ μm	*PE-flakes[b]*

Characterization (FTIR, SEM)

We used scanning electron microscopy (SEM) and Fourier transform infrared (FTIR) spectroscopy to determine morphology and chemistry of all microplastic samples.

SEM imaging was performed using a Scanning Electron Microscope SU3500 (Hitachi) with a secondary electron detector. All images, unless noted, were collected using a low 1.5 kV acceleration voltage to ensure real surface imaging at high and low magnification to characterize morphology and size, respectively. More details on the SEM methodology are provided in the Supplemental Information.

IR spectra were recorded at room temperature on a Perkin Elmer FTIR spectrometer equipped with an ATR accessory (ZeSe crystal). For each measurement, 16 scans were accumulated at a resolution of 4 cm^{-1}.

Figure 1 shows the SEM images of the samples and the corresponding chemical structure and **Figure S1** summarizes all FTIR spectra.
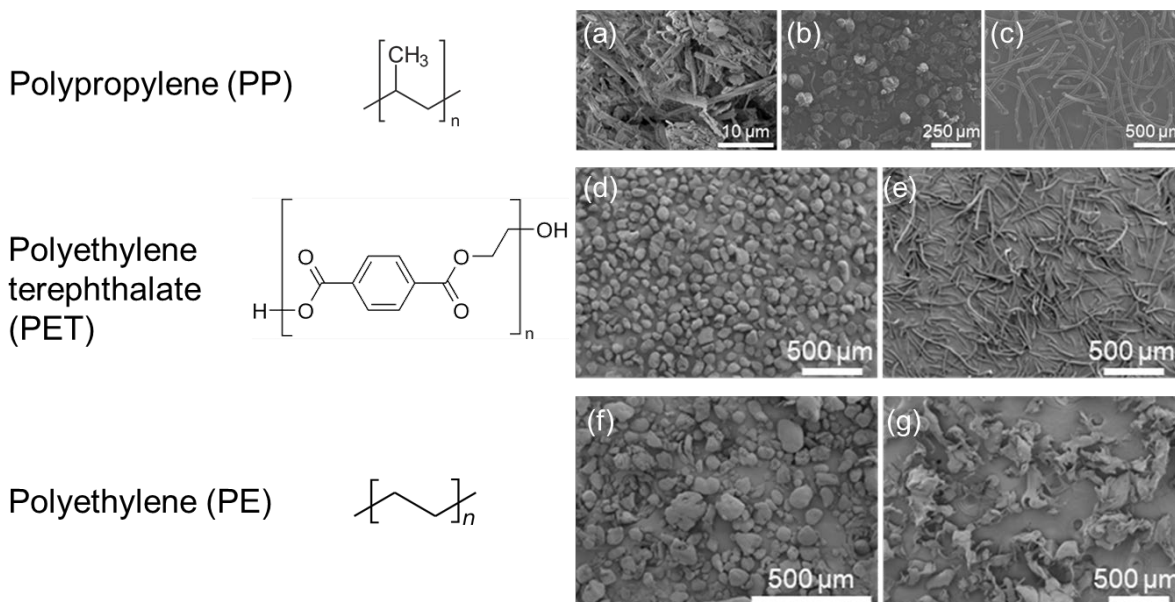

Figure 1. Chemical structures of various polymers tested for ice nucleation activity: Polypropylene (PP), polyethylene terephthalate (PET), and polyethylene (PE). Corresponding scanning microscopy images of the unaged polymer samples used in the study: (a) PP-needles[c], (b) PP-spheres[c], (c) PP-fibers[b], (d) PET-spheres[c], (e), PET-fibers[b], (f) PE-spheres[c], and (g) PE-flakes[b].

Droplet Freezing Experiments

We assessed the ice nucleation activity of the polymers using the droplet freezing technique in the immersion freezing mode.[29,30] First, we placed 20 mg of each polymer sample into a clean glass vial, followed by the addition of 10 ml of ultra-pure water (Nuclease-Free Water for Molecular Biology; Sigma-Aldrich, Burlington, MA, USA) to create a stock suspension. Next, we sonicated the samples for 5 min to disperse the microparticles in the ultra-pure water. For ice nucleation measurements, we first cleaned three siliconized glass slides (18 mm, HR3-239; Hampton Research, Aliso Viejo, CA, USA) with MilliQ water (specific resistivity ≥ 17.5 MΩ/cm, 25°C; produced with Millipore® SAS SIMSV001, Merck Millipore, Burlington, MA, USA) and

then dried them with purified air before placing them on a cooling stage (Grant Asymptote EF600 freezer; Grant Instruments (Cambridge) Ltd, Durham, UK). As previously reported,[31] the uncertainty of temperature measurement with this droplet freezing technique is ±0.25°C. For each ice nucleation measurement, we pipetted approximately 60 droplets with a volume of 1 µL onto the glass slides. A chamber sealed the cooling stage, and a nitrogen flow of 0.2 L/min prevented condensation during cooling. The nitrogen flow exerts no influence on the freezing temperature.[30] The cold stage gradually cooled from 20°C to -30°C at a rate of 3°C/min. A camera located on the top of the chamber allowed for the real-time monitoring of the freezing process. A schematic image of the droplet freezing technique used in this study can be found elsewhere[7]. Employing a MATLAB script[32], we determined the freezing temperature of each droplet, which we then used to calculate the fraction of frozen droplets ($f_{ice}(T)$, Equation 1):

$$f_{ice}(T) = \frac{N_u(T)}{N_0} \tag{1}$$

where $N_u(T)$ represents the number of unfrozen droplets in an experiment at temperature T and N_0 the total number of droplets in an experiment.

To normalize the freezing data to the mass or surface area of the microplastics and facilitate comparison with existing literature, we calculated the number of nucleation sites per unit mass, $n_m(T)$ (Equation 2) and per surface area, $n_s(T)$ (Equation 3).

$$n_m(T) = \frac{-\ln(1 - f_{ice}(T))}{V_d} \cdot \frac{V}{m} \tag{2}$$

$$n_s(T) = n_m(T) \cdot \frac{m}{s} \tag{3}$$

V_d depicts the volume of an individual droplet, $\frac{V}{m}$ gives the reciprocal of the mass concentration of the sample suspension, and s represents the surface area of the particles.

To obtain the specific surface area of the unaged particles, we analyzed the SEM images and utilized ImageJ for all samples except for PP-needles[c]. By using the ImageJ software, we measured the diameter (and in case of fibers also the length) of at least 100 particles per sample and calculated the corresponding surface area. For these calculations, we approximated particles as spherical and fibers as cylinders. For PP-needles[c], characterized by dense, hay-like features (see **Figure 1a**), we employed N_2 sorption measurements on an ASAP 2020 gas sorption instrument (Micromeritics) to obtain the Brunauer-Emmett-Teller (BET) specific surface area[33], since obtaining identifiable, individual particles from SEM images was challenging. Before analysis, the sample was degassed for 9 h at 90°C (below sample T_m). We collected N_2 sorption data at 77 K in the relative pressure range of 0-1 (saturation pressure 1 atm), and calculated the BET surface area using the BETSI software package.[34]

Oxidation Experiments

Microplastics samples underwent exposure to O_3 in a rotating-wall flow-tube reactor (see Appendix, Figure S2).[35] A few milligrams of each microplastic sample was placed within a glass tube that was inserted inside the flow-tube reactor. The glass tube was then rotated at a fixed rate with a motor to ensure constant mixing. An ozone generator (Jelight, model: 600) produced O_3 outside the flow cell. The output from the ozone generator (2 L/min) flowed through the flow-tube reactor containing the microplastic samples. At the outlet, an O_3 monitor (Thermo Scientific, 49i) continuously monitored the O_3 concentration. We set the exposure duration for the microplastic samples at 2 h and used an O_3 concentrations of 2.8 ppmv. Background concentrations of O_3 in the planetary boundary layer (PBL) is around 30 ppbv.[36] Assuming that the aging of microplastic surfaces is proportional to both concentration and time, the exposures in our experiment correspond to 7.7 days at 30 ppbv.

In addition, we performed aging experiments using a commercial UV-ozone cleaning device (ProCleaner™, Bioforce Nanosciences). We put a thin layer of each microplastic sample onto the sample stage within the oxidation chamber. The cleaning device generates UVC light (185 nm and 254 nm) using a mercury lamp. **Figure S3** in the Supplement Information depicts the irradiance spectrum of the mercury lamp used in the chamber. Also, 185 nm light generates O atoms and O_3 by reactions (1) and (2)[37]:

$$O_2 + h\nu(185 \text{ nm}) \rightarrow 2\, O(^3P) \tag{1}$$

$$O(^3P) + O_2 + M \rightarrow O_3 + M \tag{2}$$

In addition, 254 nm light generates hydroxyl radicals (OH) in the presence of water vapor by reactions (3) and (4)[37,38]:

$$O_3 + h\nu(254 \text{ nm}) \rightarrow O(^1D) + O_2 \tag{3}$$

$$O(^1D) + H_2O \rightarrow 2 \cdot OH \tag{4}$$
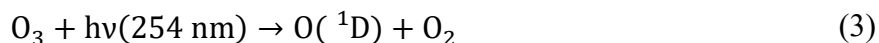
O_3 concentrations generated in these experiments reached 5.9 ppmv. The exposure of microplastics to these aging conditions lasted 2 h. To ensure uniform treatment of light and O_3 throughout the entire sample, we opened the chamber every approx. 15 min, and thoroughly mixed the samples manually. The O_3 exposures in these experiments correspond to 16.3 days at 30 ppbv (background PBL conditions). The exposure to 185 nm and 254 nm light in these experiments are upper limits to exposure in the troposphere, since most of these wavelengths are filtered out by the ozone layer in the stratosphere. The OH concentrations in these experiments were not measured, but OH concentrations are two or three orders of magnitude higher than observed in the atmosphere and can be produced using the same wavelengths and a similar configuration.[39] Assuming OH concentrations two orders of magnitude higher than ambient, the OH exposures correspond to roughly 200 hours or 8.3 days under ambient conditions. Until additional data is available, these

aging experiments with UVC and O_3, should be considered as upper limits to aging in the troposphere. Additional studies are needed with a combination of UV and O_3 exposures typical of the troposphere.

Following both oxidation experiments, we transferred 20 mg from each treated microplastics sample into a sterile glass tube, added 10 ml of ultra-pure water, sonicated for a duration of 5 min, and then measured ice nucleation activity (triplicates at minimum).

Results and Discussion

Freezing results for unaged microplastics

Freezing curves in **Figure 2** reveal that three suspensions of microplastic samples (PP-needles[c], PP-fibers[b], and PET-fibers[b]) froze at temperatures above the water blank, indicating a heterogeneous freezing process. The T_{50} (i.e. the temperature at which 50 % of the droplets were frozen) values for these three suspensions were -20.88°C ± 0.52 for PP-needles[c], -23.24°C ± 0.21 for PP-fibers[b], and -21.93°C ± 0.51 for PET-fibers[b], compared to -25.78°C ± 1.21 for the water blank. **Table 2** summarizes all T_{50}-values including 83% confidence intervals.
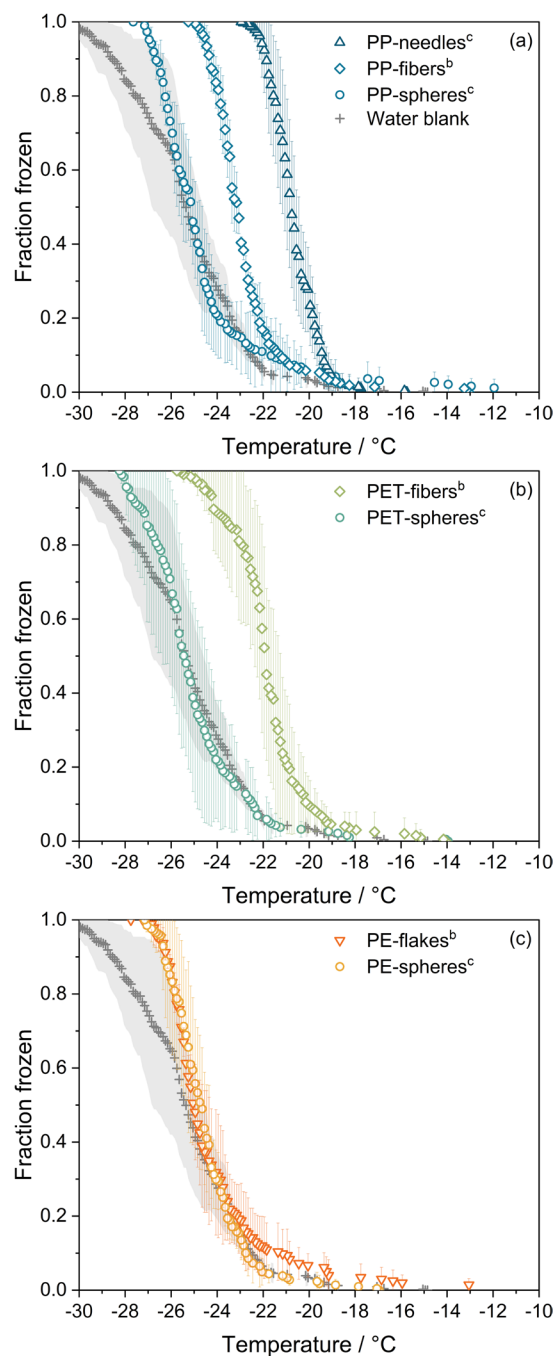
Figure 2. Fraction of frozen droplets in dependence of temperature ($f_{ice}(T)$) for seven microplastic suspensions (2.0 x 10^{-2} wt%) and the water blank. (a) Polypropylene (PP) needles[c], fibers[b] and spheres[c], (b) polyethylene terephthalate (PET) spheres[c] and fibers[b], and (c) polyethylene (PE) spheres[c] and flakes[b]. In all plots the water blank is depicted in grey. The error bars of the samples and blank represent the 83% confidence interval. Two datasets are statistically distinct with a 95% confidence level if their respective 83% confidence bands do not overlap.[40] Experiments were performed in triplicate at minimum.

The freezing curves of PP-spheres[c], PET-spheres[c], PE-spheres[c], and PE-flakes[b] fall within the confidence interval of the water blank freezing curve and are therefore not distinguishable from the background. However, the freezing curves of these plastic samples deviate from the mean of the blank at fraction frozen values close to 1, which could indicate that some heterogeneous activity may exist. Given that freezing of the water background in μL-sized droplet freezing assays, as used in this study, is typically around -25°C[30], evaluating particle-induced freezing below this temperature would require an alternative assay using droplets in the nL range, where background freezing occurs around -35°C.[41]

To normalize the freezing data to the mass and surface area and compare our data with the literature, we determined the number of nucleation sites per unit mass, $n_m(T)$, and surface area, $n_s(T)$, (**Figure 3**). The $n_m(T)$ values of the different ice-active microplastics samples agree within about one order of magnitude and increase roughly exponentially as temperature decreases (**Figure 3a**). At -18°C the values range from 7.2 x 10^4 to 1.5 x 10^5 g^{-1}, and at -22°C the values range from 9.0 x 10^5 to 1.3 x 10^7 g^{-1}. The following order was observed at a freezing temperature of -22°C: PP-needles[c] > PET-fibers[b] > PP-fibers[b]. The $n_s(T)$ values of all ice-active microplastics agree within about two orders of magnitude and increased roughly exponentially with decreasing temperature (**Figure 3b**). At -18°C the $n_s(T)$ values range from 4.5 x 10^{-1} to 8.7 x 10^1 cm^{-2}, and at -22 °C the values range from 8.0 x 10^1 to 2.1 x 10^3 cm^{-2}. In general, the following order was observed PET-fibers[b] $\cong$ PP-fibers[b] > PP-needles[c].

Our dataset highlights the variability in ice nucleation behavior among microplastic particle types. The reason for this variably is not clear. Knowledge of the polymer type is insufficient to predict whether nucleation will occur. For example, the $n_s(T)$ values for PP-fibers[b] were higher

than the $n_s(T)$ values for PP-needles[c]. PP can be subdivided into atactic (randomly aligned methyl groups, CH_3), syndiotactic (alternating CH_3 groups), and isotactic (evenly distributed CH_3 groups) structures. These structural variances impact crystallinity (amorphous or semi-crystalline), which could modify ice nucleation ability. Additives can also be introduced by companies during production, which can lead to variations in morphology and surface properties, which could also modify ice nucleation ability.

FTIR analysis (**Figure S1**) revealed that PP-needles[c] possessed oxygen-containing functional groups despite PP being a polyolefin. Notably, the PP-needles[c] exhibited the highest nucleation temperature among all tested microplastics (see **Figure 1**), prompting initially speculation about a potential link between oxygen content, oxidation, and ice nucleation activity. However, we did not see a clear correlation between the oxygen content of the unaged microplastics (see **Figure S1**) and the ice nucleation ability. For example, PET-spheres[c] had a high oxygen content (**Figure S1**) but did not induce ice nucleation in our experiments.

Two out of three of the ice-active microplastics were generated by the breakdown of frequently used commercial products (PP-fibers[b] and PET-fibers[b]) (**Figure 2**). This result may suggest that the breakdown of microplastics may generate ice nucleation sites. Possibly related, previous work has shown that grinding minerals lead to an increase in ice nucleation sites.[8,42] Nevertheless, not all the microplastics generated by the breakdown of frequently used commercial products were ice-active. Specifically, PE-flakes[b] was not ice-active. Hence, breakdown of microplastics was the not the only factor controlling ice nucleation in our experiments.
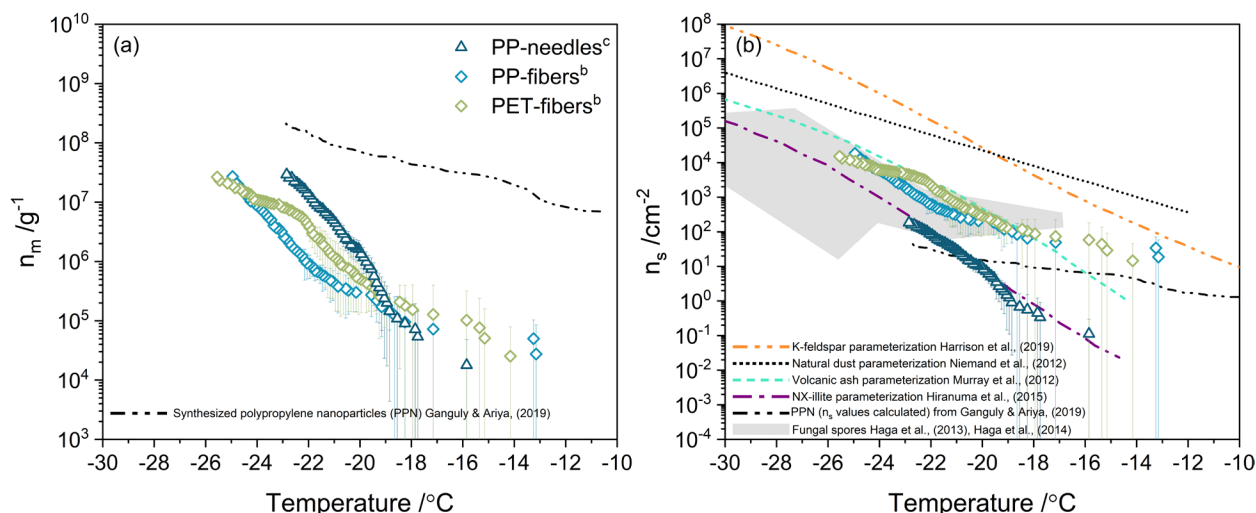
Figure 3. Ice nucleation active site densities normalized to **(a)** mass and **(b)** surface of polypropylene (PP) needles[c], PP-fibers[b], and polyethylene terephthalate (PET) fibers[b]. Error bars denote the 83% confidence intervals of $n_m(T)$ and $n_s(T)$ at temperature T calculated using Student's t-distribution. Two datasets are statistically distinct with a 95% confidence level if their respective 83% confidence bands do not overlap.[40] Literature data of n_m values from PP nanoparticles are shown from Ganguly and Ariya[19] in black (dash-dot-dot). Literature values of n_s parameterizations are shown for comparison: K-feldspar from Harrison et al.[43] (orange dash-dot-dot), natural dust from Niemand et al.[44] (black dots), volcanic ash from Murray et al.[45] (turquoise dash), and NX-illite from Hiranuma et al.[46] (purple dash-dot). $n_s(T)$ values of PP nanoparticles (PPN) were calculated from data obtained from Ganguly and Ariya[19] (black dash-dot-dot). The grey area depicts $n_s(T)$ values from fungal spores by Haga et al.[47] and Haga et al.[6].

Comparison of the freezing results for unaged microplastics with literature data

Ganguly and Ariya[19] synthesized three microplastics types (PP, low-density PE, and high-density PE) in the laboratory and quantified their freezing properties using a droplet freezing technique. In **Figure 3a**, we have compared our freezing results with their PP microplastics. Our observed $n_m(T)$ data are lower than the literature values by 1-4 orders of magnitude for freezing temperatures between -16 and -22°C. We calculated $n_s(T)$ values by computing them from the $n_m(T)$ values reported by Ganguly and Ariya[19] using an average diameter of 193 nm for their

microplastics, which corresponds with their own measurements. Using this approach, the calculated $n_s(T)$ values based on the data from Ganguly and Ariya[19] closely match our microplastics data (**Figure 3b**). This suggests that the difference in $n_m(T)$ values between our study and Ganguly and Ariya[19] can be attributed to differences in the surface area used in the experiments, rather than a significant variance in the ice nucleation ability per unit surface area.

To help put the freezing ability of microplastics into context, the ice nucleation active surface-site densities, $n_s(T)$, of the PP-needles[c], PP-fibers[b], and PET-fibers[b] were compared to those for volcanic ash[45], fungal spores, NX-illite[46], K-feldspar[43], and a natural mineral dust[44] parameterizations (see **Figure 3b**). The ice nucleation properties of mineral dust and volcanic ash have been the focus of many studies, and both represent important types of INPs in the atmosphere. NX-illite consists of illite (main component with 74 wt%[48,49]), kaolinite, quartz, calcite, and feldspars and has been used as a proxy for mineral dust INPs.[46] Mineral dust and volcanic ash are both important types of INPs in the atmosphere, and their ice nucleation ability has been the focus of many studies. K-feldspar is one of the most effective types of mineral dust INPs and has been incorporated into models of atmospheric INPs.[50] Fungal spores have been found in atmospheric aerosol and cloud water samples and shown to nucleate ice.[51] The $n_s(T)$ values for PP-needles[c], PP-fibers[b], and PET-fibers[b] are comparable to those for volcanic ash[45], NX-illite[46] and fungal spores[6,47]. On the other hand, the $n_s(T)$ values for the same microplastics are approximately 2-3 orders of magnitude lower than those for K-feldspar[43] and a parameterization for natural mineral dust[44]. K-feldspar and natural mineral dust are considered highly effective INPs.

Possible effects of unaged microplastics on clouds and long-range transport.

A recent study by González-Pleiter et al.[52] showed that microplastics, specifically polymer fragments and artificial fibers, can accumulate to concentrations reaching up to 0.032 L^{-1} in the

PBL above urban areas.[46] The identified fibers exhibited an average length and width of 662 μm and 25.4 μm, respectively, similar to PP-fibers[b] in our study. To provide an initial assessment of the potential impact of microplastics on clouds, we combined the upper limit of microplastics concentrations reported by González-Pleiter et al.[52] (0.032 L^{-1}) and our freezing results for the PP-fibers[b]. First, we calculated the number of ice nucleation sites per fiber at a freezing temperature of -20°C using the freezing data for PP-fibers[b] and the following equation:

$$IN \ per \ fiber(-20°C) = \frac{-\ln\big(1 - f_{ice}(-20°C)\big)}{V_d} \div \frac{fibers}{droplet} \tag{4}$$

$Fibers/droplet$ was determined based on the average volume of the individual PP-fibers[b] and a density of 0.90 g/cm^3.[54] The calculation using Equation 4 gave 0.15 ice nucleation sites per fiber at -20°C. Next, we used this value along with the microplastic concentrations reported by González-Pleiter et al.[52] (0.032 L^{-1}) to estimate an INP concentration of 0.005 L^{-1} of air at a freezing temperature of -20 °C. Previous studies have shown that an INP concentration of 0.01 L^{-1} of air at -20°C can be sufficient to influence cloud glaciation.[55] Hence, we conclude that in some situations over urban areas and in the PBL, microplastics may influence cloud glaciation. Nevertheless, more studies like those by González-Pleiter et al.[52] are needed to determine the concentrations of microplastics in the atmosphere, especially at altitudes where mixed-phase clouds occur. Additional studies are also needed to fully characterize the ice nucleation properties of microplastics that are emitted to the atmosphere. In addition, our analysis did not consider the presence of mineral dust INPs and biological INPs in the atmosphere, which can cause ice nucleation at warmer temperatures than microplastic INPs and limit the effect of microplastics INPs on cloud glaciation. Additional studies are needed to consider these competing effects.

   If the microplastics nucleate ice (as shown here for certain types of microplastics) ice nucleation followed by precipitation can also affect the long-range transport and atmospheric concentrations

of microplastics. Recent modelling studies show that ice nucleation by fungal spores followed by precipitation, significantly impacted the long-range transport and concentrations of fungal spores in remote regions and the upper troposphere.[6] The size of fungal spores range from 2 to 50 μm.[56] Since some microplastics have similar n_s values to fungal spores (**Figure 3b**), and may have similar sizes to some fungal spores, ice nucleation by microplastics may influence their long-range transport and concentrations in remote regions and the upper troposphere under some atmospheric conditions, such as when mineral dust and biological INP concentrations are low. The freezing data included here provide necessary information for including this phenomenon into atmospheric models.

Freezing results for aged microplastics

When suspended in the air, microplastics undergo atmospheric aging due to exposure to oxidants (e.g. O_3) and UV light, which can change their chemical and physical properties, including ice nucleating properties. To investigate the effect of atmospheric aging on the ice nucleation activity of microplastics, we exposed the microplastics to O_3 using a flow-tube reactor and investigated change in ice activity. The O_3 exposures in our experiments corresponded to 16.3 days at 30 ppbv (background PBL conditions). We also conducted UVC+O_3 experiments to simulate an upper limit to photooxidation in the troposphere. **Figure 4** shows the freezing curves in the form of boxplots before and after the aging experiments, and **Table 2** summarizes all T_{50} values including 83% confidence intervals before and after oxidation experiments.
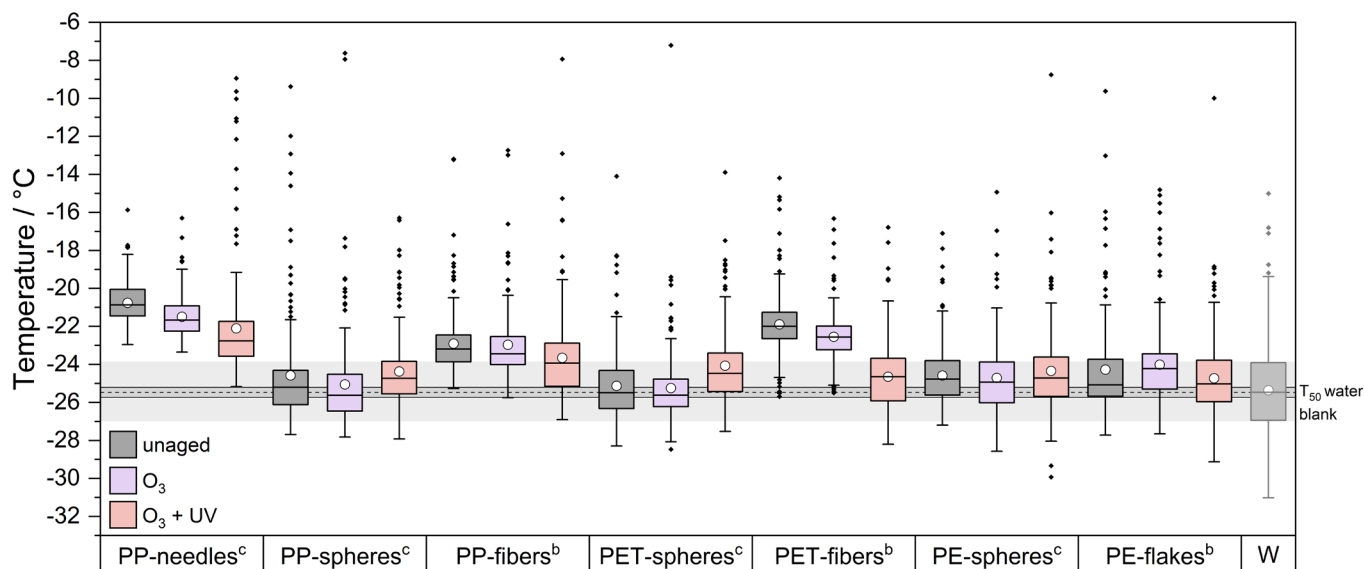
Figure 4. Freezing curves ($f_{ice}(T)$), represented by boxplots, of the seven microplastics samples (polypropylene (PP) needles[c], spheres[c], and fibers[b]; polyethylene terephthalate (PET) spheres[c] and fibers[b]; polyethylene (PE) spheres[c] and flakes[b]) before and after oxidation experiments. Within each sample type, the first box represents the unaged sample (grey box), followed by post-ozone (O_3) exposure (depicted in purple), and post UVC+O_3 (i.e. photooxidation) exposure (highlighted in red). Each box contains cumulative data from at least three replicates. The upper and lower limit of the box represents the interquartile range (25th and 75th percentiles), the median (T_{50}) is displayed as a vertical line within the box, and the black rectangle signifies the mean value. Whiskers extend to the 5th and 95th percentiles, while outliers are identified as diamonds. The light grey boxplot to the right represents the water blank. The dashed line throughout the graph indicates the T_{50} value of the blank, the dark grey area denotes the corresponding standard error of T_{50}, and the light grey area illustrates the interquartile range.

Table 2.: T_{50} values of microplastics suspension samples and water blank with 83% confidence intervals. Two datasets are statistically distinct with a 95% confidence level if their respective 83% confidence bands do not overlap[40].

Sample	unaged		after O$_3$		after UVC+O$_3$	
	T_{50} /°C	$CI_{83\%}$/°C	T_{50} /°C	$CI_{83\%}$/°C	T_{50} /°C	$CI_{83\%}$/°C
PP-needles[c]	-20.88	0.43	-21.70	0.06	-22.76	0.23
PP-spheres[c]	-25.21	0.53	-25.60	0.27	-24.79	0.60
PP-fibers[b]	-23.24	0.22	-23.46	0.13	-23.87	0.69
PET-spheres[c]	-25.54	1.19	-25.67	0.41	-24.48	0.31
PET-fibers[b]	-21.93	0.54	-22.63	0.22	-24.80	0.86
PE-spheres[c]	-24.83	0.63	-24.94	0.95	-24.72	0.33
PE-flakes[b]	-24.89	0.55	-24.31	0.51	-25.09	0.46
Blank	-25.78	1.01				

Overall, exposure to O$_3$ or UVC+O$_3$ (referred to as photooxidation hereafter) either caused no change (i.e. the change was less than the uncertainties of the measurements) or a decrease in ice nucleation activity. For the non-ice nucleation active plastics (PP-spheres[c], PET-spheres[c], PE-spheres[c], PE-flakes[b]) no statistically significant change in ice nucleation activity was observed after exposure to O$_3$ or photooxidation. A similar result was observed for the ice-active sample PP-fibers[b] (i.e. no change was observed). On the other hand, for the ice nucleation active samples PP-needles[c] and PET-fibers[b], nucleation temperatures decreased slightly after exposure to O$_3$ and more strongly after photooxidation.

We conclude that atmospheric aging due to O$_3$ exposure and photooxidation can lead to reduction in the ice nucleation ability of some microplastics, but not all. These results are consistent with previous studies that showed exposure to O$_3$ or other oxidants lead to either no

change or a decrease in ice nucleation ability of some atmospherically relevant organic particles and material, such as lignin[57] and pollen[58]. Soot particles aged with O_3 also did not show enhanced ice nucleation ability.[59,60] In contrast, studies on inorganic mineral dusts (Arizona test dust and kaolinite) have revealed an enhancement in ice nucleation ability after exposure to O_3.[61]

We employed FTIR and SEM measurements to track chemical and morphological alterations due to exposure to O_3 and photooxidation. Results are shown in **Figure S4** to **Figure S9**. In **Table 3**, we summarize the observed changes in the chemical and physical properties of the ice-active microplastics (PP-fibers[b], PP-needles[c], and PET-fibers[b]) due to exposure to O_3 and photooxidation. For comparison purposes, the change in ice nucleation activity with O_3 exposure and photooxidation are also included in **Table 3**.

O_3 exposure did not cause a detectable change in the chemical or morphological properties of the ice-active microplastics (PP-fibers[b], PP-needles[c], and PET-fibers[b]) (**Table 3**, column 3 and column 4). On the other hand, O_3 exposure caused a decrease in ice nucleation ability of the PP-needles[c] and PET-fibers[b] (**Table 3**, column 2). We conclude that O_3 exposure must have caused some chemical and/or physical changes at the surface of the PP-needles[c] and PET-fibers[b] that were not detected with FTIR or SEM measurements. Future studies that use surface-focused analytical techniques are needed to understand the relationship between O_3 exposure and ice nucleation ability of microplastics.

Photooxidation caused an increase in oxygen-containing functional groups for PP-needles[c] and PP-fibers[b], but not PET-fibers[b] (**Table 3**, column 6). On the other hand, photooxidation caused a decrease in ice nucleation activity for PP-needles[c] and PET-fibers[b], but not PP-fibers (**Table 3**, column 2). We conclude that the decrease in ice nucleation ability caused by photooxidation cannot be explained by just the increase in oxygen-containing functional groups observed with FTIR

spectroscopy. Photooxidation also caused a change in morphology (formation of cracks) for PP-fibers[b], but not PP-needles[c] and PET-fibers[b] (**Table 3**, column 7). We conclude that the decrease in ice nucleation ability caused by photooxidation cannot be explained by just a change in morphology observed with SEM since a change in ice nucleation activity did not correlate with a change in morphology. These results also underscore the need for surface-focused analytical techniques to explain the relationship between photooxidation and ice nucleation ability of microplastics.

Table 3. Summary of the effect of O_3 exposure and photooxidation on ice nucleation activity, chemistry and morphology of ice-active microplastic samples. Text highlighted in bold and red indicate that a significant change was observed.

Sample	O₃ exposure			Photooxidation (UVC+O₃)		
	Δ IN activity	*Δ chemistry*	*Δ morphology*	*Δ IN activity*	*Δ chemistry*	*Δ morphology*
PP-needles[c]	**Decrease**	No detectable change	No detectable change	**Decrease**	**Surface and/or bulk oxidation**	No detectable change
PP-fibers[b]	No detectable change	No detectable change	No detectable change	No detectable change	**Surface and/or bulk oxidation**	**Formation of cracks**
PET-fibers[b]	**Decrease**	No detectable change	No detectable change	**Decrease**	No detectable change	No detectable change

The influence of microplastics on atmospheric processes, notably their potential influence on ice nucleation in clouds, remains a subject of uncertainty. Our results demonstrate that certain microplastic samples, specifically PP-needles[c], PP-fibers[b], and PET-fibers[b] heterogeneously nucleate ice in the immersion freezing mode at temperatures between -15 and -25°C and have

$n_s(T)$ values similar to fungal spores and volcanic ash. Exposure to O_3 and $UVC+O_3$ led to a reduction in nucleation temperature for two (PP-needles[c] and PP-fibers[b]) out of the three ice-active microplastics. Our results are consistent with field measurements by Kozjek et al.[62] who observed fibrous microplastics inside hailstones.[62] Since the mid-20th century, our environment has been increasingly inundated with plastics. Considering the time lag from the release of plastics into the environment to their gradual transformation into microplastics, it is likely that the concentration of microplastics will continue to rise in the future and play a more significant role in ice formation in the atmosphere.

ACKNOWLEDGMENT

AUTHOR INFORMATION

Corresponding Author

*Allan K. Bertram, bertram@chem.ubc.ca

Author Contributions

T.M.S. prepared the manuscript with contributions from all authors. T.M.S. and A.K.B. designed the project. T.M.S. performed the ice nucleation experiments. T.M.S. and S.N. performed oxidation experiments. A.M.M. conducted SEM measurements. L.J.A. collected BET data. E.R.G. and A.K.B. supervised the project.

Supporting Information

SEM measurements

Each dry microplastic sample was deposited on individual aluminum SEM stubs (25 mm diameters, Item 1614-9, TED PELLA) coated with an adhesive carbon tape. To ensure proper particle distribution throughout the stub, approx. 1 mg of each sample was dispersed with a micro-spatula onto a glass slide and picked up by gently pressing the stub with the carbon tape against the slide and picking up adhered particles. Afterwards, samples' stubs were sputter coated with 10 nm Iridium using an EM MED020 Coating System (Leica). Imaging was recorded with a Scanning Electron Microscope SU3500 (Hitachi) using a secondary electron detector. Images were acquired using a 1.5 kV acceleration voltage, except for PP-needles[c] after O_3 and UVC+O_3, for which a 10 kV acceleration voltage was employed.

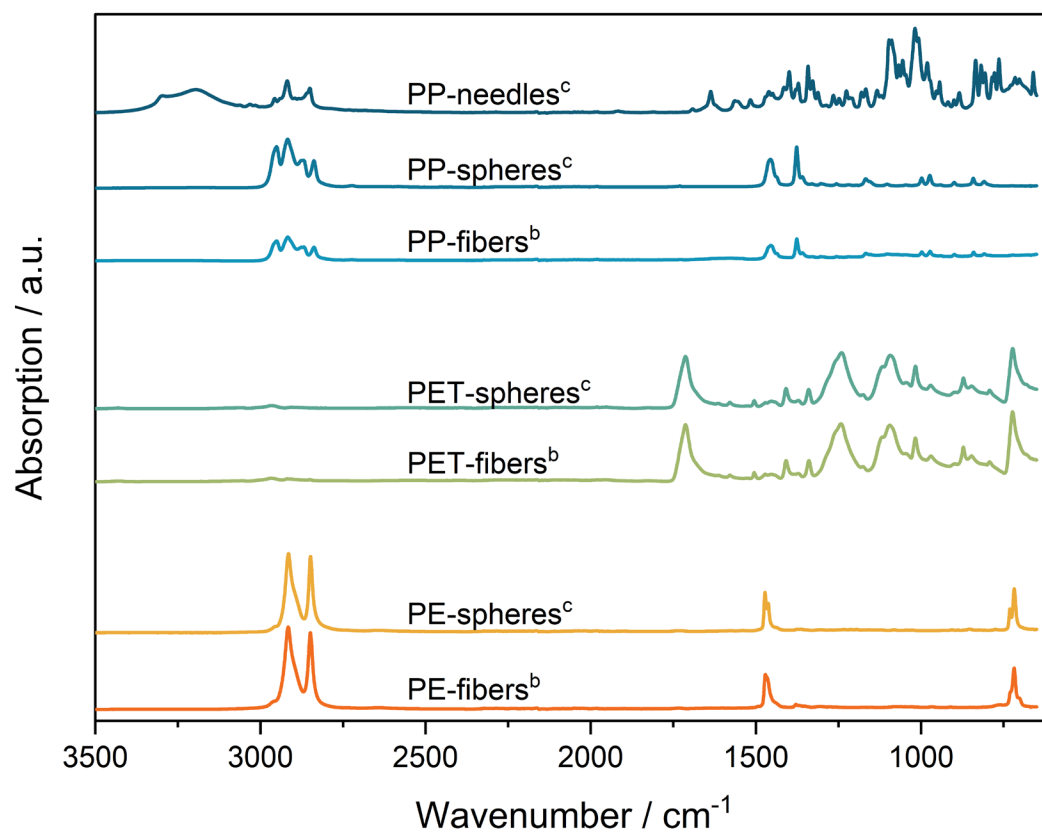# FTIR spectra of unaged microplastic samples

Figure S1. FTIR spectra of all unaged polymer samples studied in this project. PP corresponds to polypropylene, PET to polyethylene terephthalate, and PE to polyethylene.
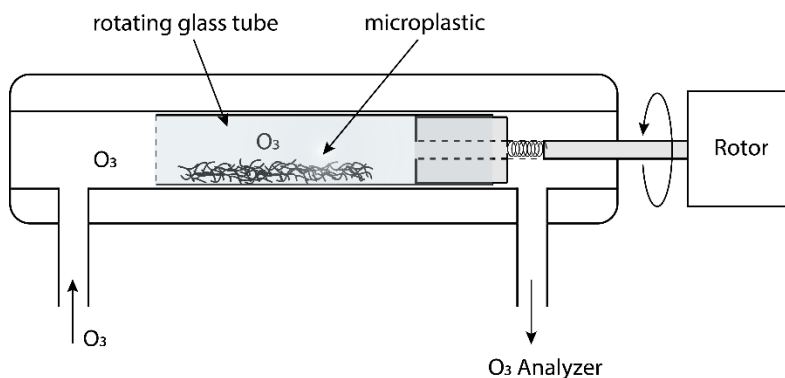
Rotating-wall flow-tube reactor

Figure S2: Schematic diagram of the rotating-wall flow-tube reactor for the ozone (O_3) exposure experiments with the microplastic samples. The sample was placed in a pre-cleaned glass cylinder (rotating glass tube) connected to a rotating motor. The ozone flows through the reactor and the concentration is measured at the outlet.
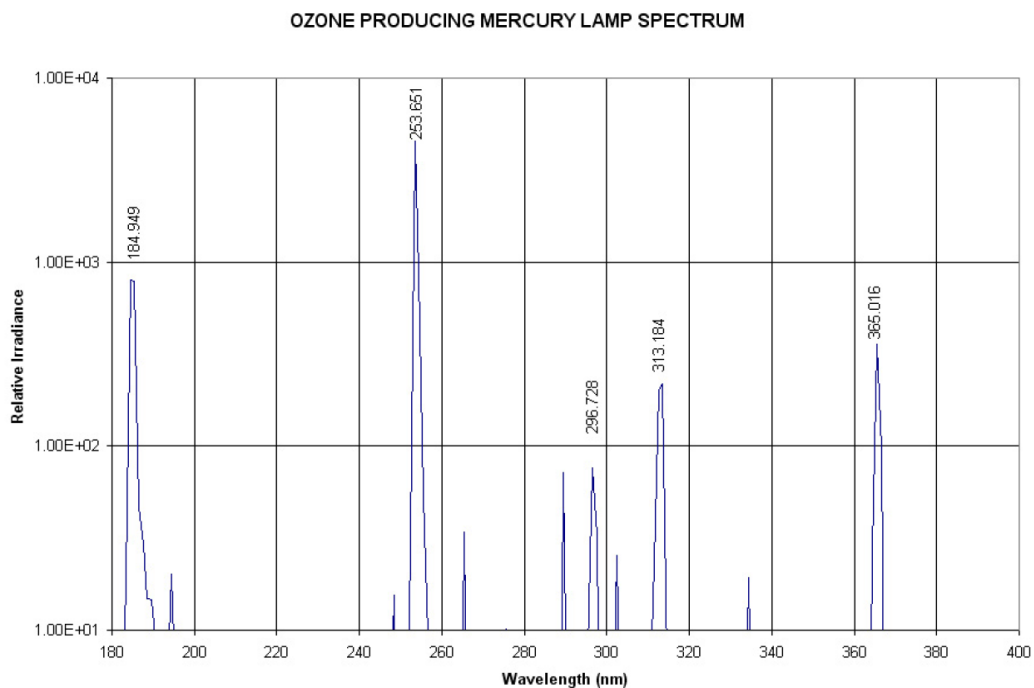
Mercury lamp spectrum

Figure S3. Irradiance spectrum of the UV lamp as a function of wavelength. Provided by BioForce Nanoscience Inc.

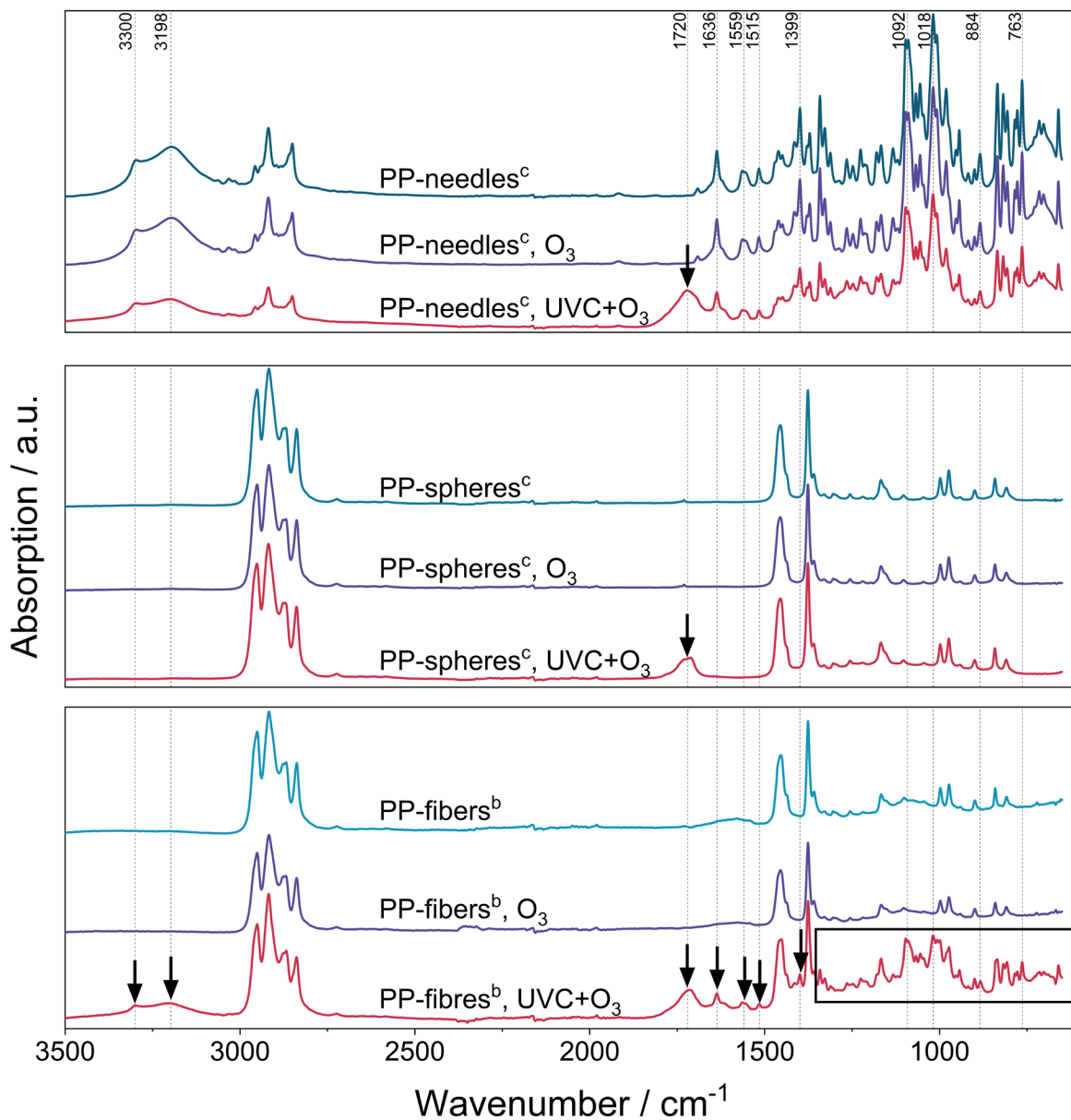## FTIR spectra of unaged and aged microplastic samples

Figure S4. FTIR spectra of polypropylene (PP) microplastics samples before, after O_3 oxidation, and after photooxidation (UVC+O_3). Spectra were recorded from the dry samples (before making solutions for ice nucleation measurements). Arrows denote alterations after oxidation experiments. Peak assignments are listed in Table S1.

Table S1: Selected IR bands visible in FTIR spectra of polypropylene samples after oxidation experiments (see Figure S4).

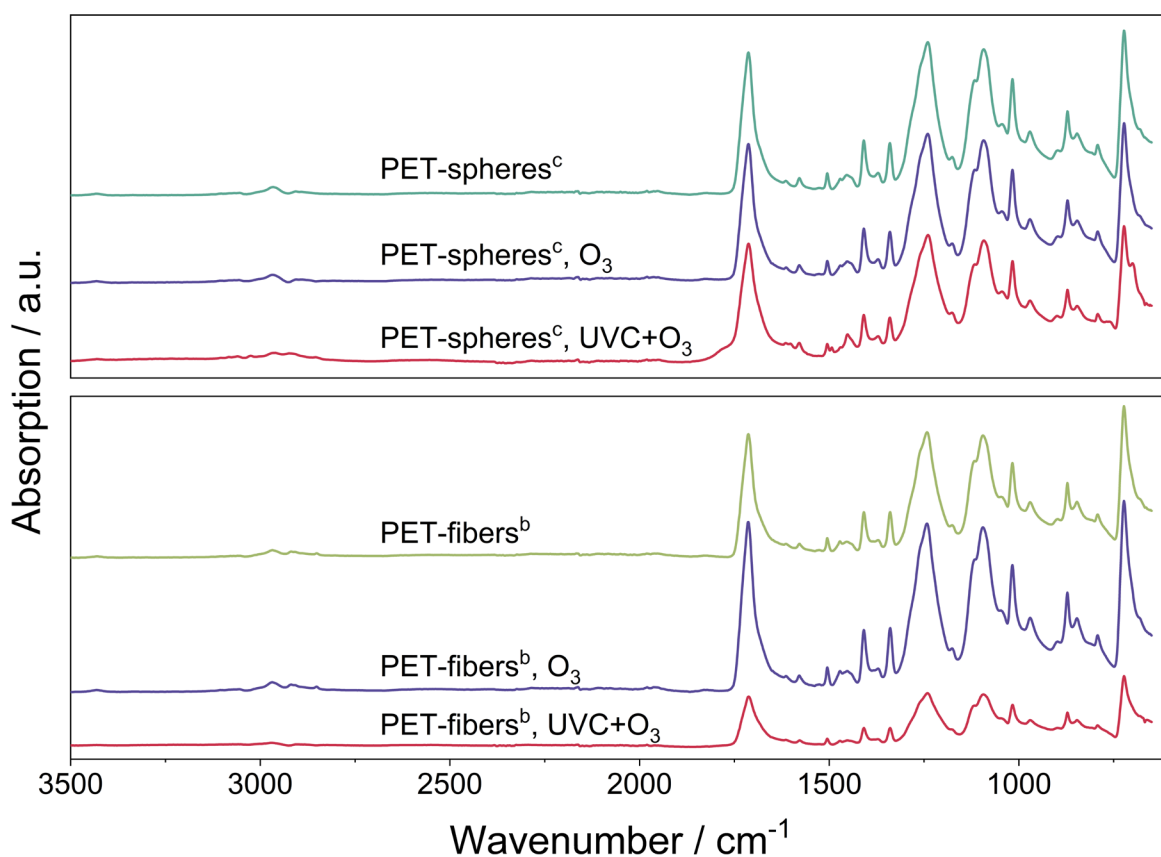| Band wavenumber(cm^{-1})	Assignment of IR spectra
3300	R-O-O-H
3198	O-H stretch
1720	C=O stretch
1636, 1559	C=C
1092	C–C stretch, CH_2 wag, CH twist
1018	C–C bend, CH_3 rock, CH bend, C–O–C, ether

Figure S5. FTIR spectra of polyethylene terephthalate (PET) microplastics samples before, after O_3 oxidation, and after photooxidation (UVC+O_3). Spectra were recorded from the dry samples (before making solutions for ice nucleation measurements).

Figure S6. FTIR spectra of polyethylene (PE) microplastics samples before, after O_3 oxidation, and after photooxidation (UVC+O_3). Spectra were recorded from the dry sample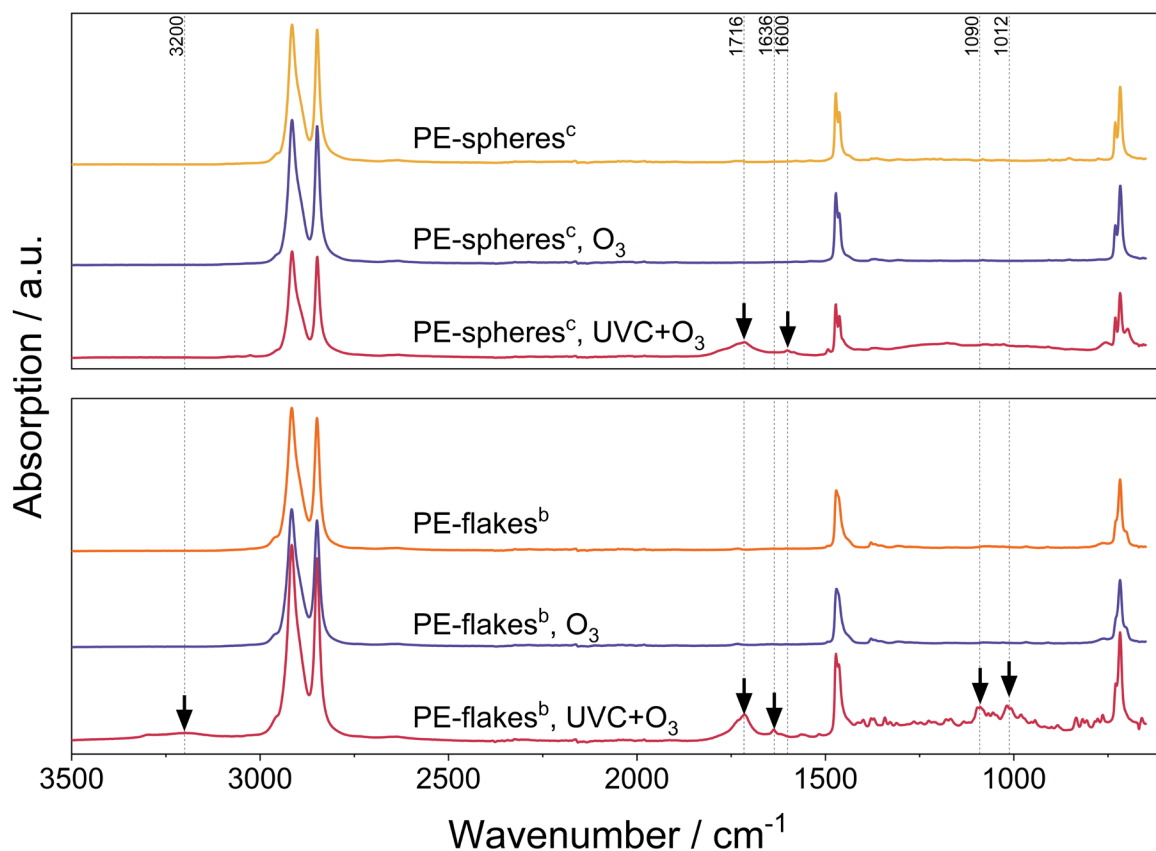s (before making solutions for ice nucleation measurements). Arrows denote alterations after oxidation experiments. Peak assignments are listed in Table S2.

Table S2: Selected IR bands visible in FTIR spectra of polyethylene samples after oxidation experiments (see Figure S6).

Band wavenumber (cm^{-1})	Assignment of IR spectra
3200	O–H stretch
1716	C=O
1600-1680	C=C
1100	secondary alcohols, ketones

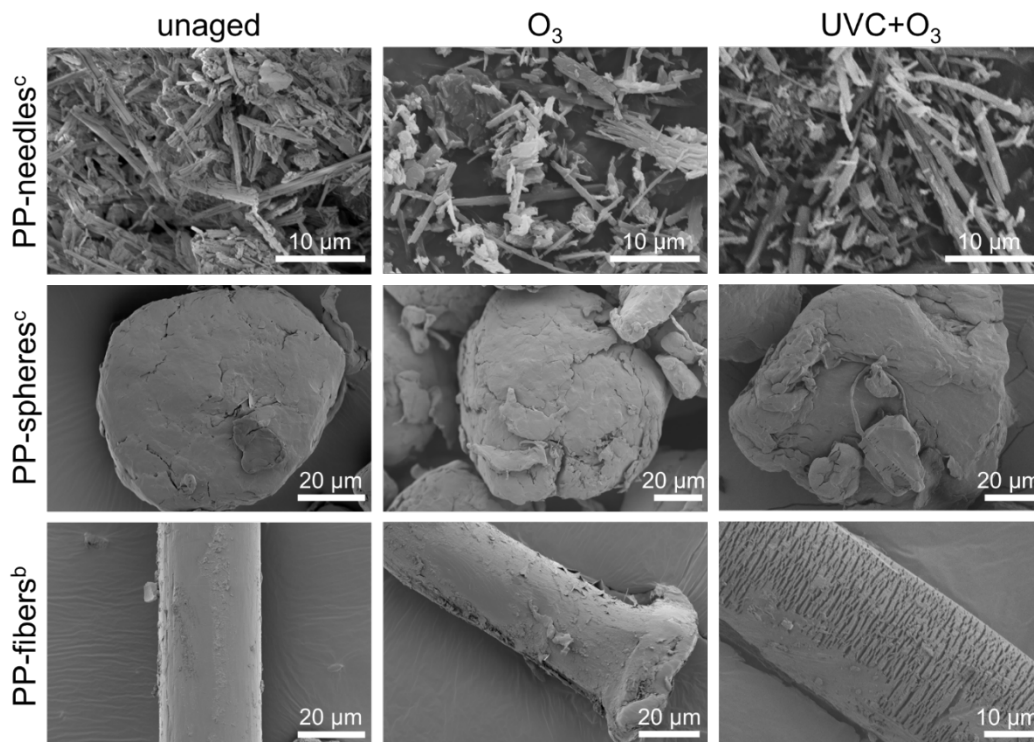# SEM images of unaged and aged microplastic samples

Figure S7. SEM images of polypropylene (PP) needles, spheres, and fibers: unaged, after exposure to O_3, and photooxidation (UVC+O_3).
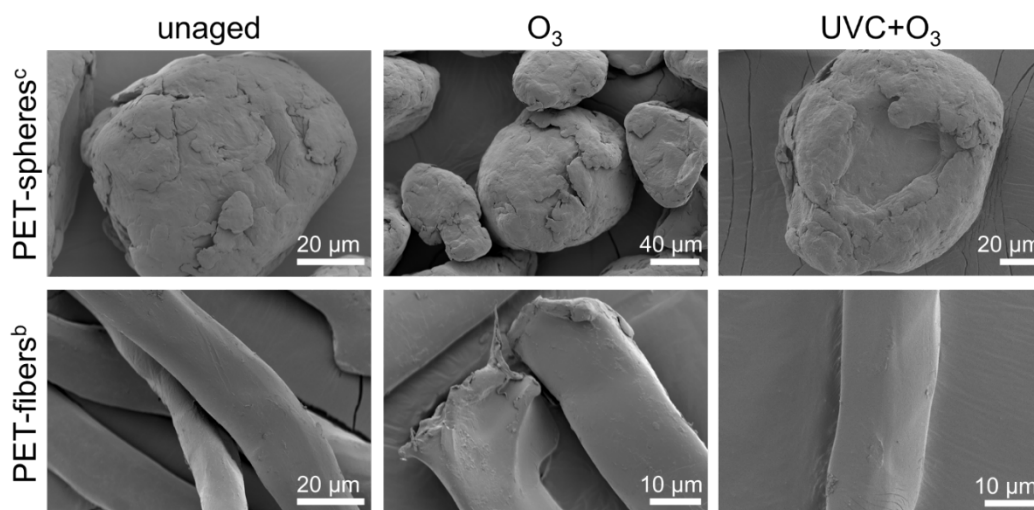

Figure S8. SEM images of polyethylene terephthalate (PET) spheres and fibers: unaged, after exposure to O_3, and photooxidation (UVC+O_3).
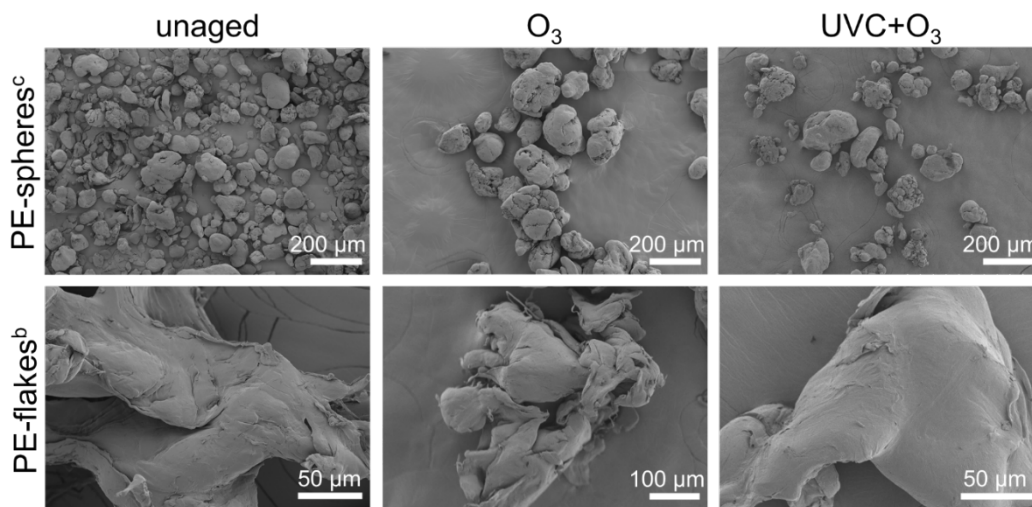
Figure S9. SEM images of polyethylene (PE) spheres and flakes: unaged, after exposure to O_3, and photooxidation (UVC+O_3).

REFERENCES

(1)   Pruppbacher, H. R.; Klett, J. D. Homogeneous Nucleation of Ice in Supercooled Water. In *Microphysics of Clouds and Precipitation*; Kluwer Academic Publishers, 1997; p 954.

(2)   Koop, T.; Murray, B. J. A Physically Constrained Classical Description of the Homogeneous Nucleation of Ice in Water. *J. Chem. Phys.* **2016**, *145* (21), 211915. https://doi.org/10.1063/1.4962355.

(3)   Korolev, A.; Isaac, G. Phase Transformation of Mixed-Phase Clouds. *Q. J. R. Meteorol. Soc.* **2003**, *129* (587), 19–38. https://doi.org/10.1256/qj.01.203.

(4)   Mülmenstädt, J.; Sourdeval, O.; Delanoë, J.; Quaas, J. Frequency of Occurrence of Rain from Liquid-, Mixed-, and Ice-Phase Clouds Derived from A-Train Satellite Retrievals. *Geophys. Res. Lett.* **2015**, *42* (15), 6502–6509. https://doi.org/10.1002/2015GL064604.

(5)   Lohmann, U.; Feichter, J. Global Indirect Aerosol Effects: A Review. *Atmos. Chem. Phys.* **2005**, *5* (3), 715–737. https://doi.org/10.5194/acp-5-715-2005.

(6)   Haga, D. I.; Burrows, S. M.; Iannone, R.; Wheeler, M. J.; Mason, R. H.; Chen, J.; Polishchuk, E. A.; Pöschl, U.; Bertram, A. K. Ice Nucleation by Fungal Spores from the Classes Agaricomycetes, Ustilaginomycetes, and Eurotiomycetes and the Effect on the Atmospheric Transport of These Spores. *Atmos. Chem. Phys.* **2014**, *14* (16), 8611–8630. https://doi.org/10.5194/acp-14-8611-2014.

(7)   Worthy, S. E.; Kumar, A.; Xi, Y.; Yun, J.; Chen, J.; Xu, C.; Irish, V. E.; Amato, P.; Bertram, A. K. The Effect of (NH$_4$)$_2$SO$_4$ on the Freezing Properties of Non-Mineral Dust Ice-

Nucleating Substances of Atmospheric Relevance. *Atmos. Chem. Phys.* **2021**, *21* (19), 14631–14648. https://doi.org/10.5194/acp-21-14631-2021.

(8)   Zolles, T.; Burkart, J.; Häusler, T.; Pummer, B.; Hitzenberger, R.; Grothe, H. Identification of Ice Nucleation Active Sites on Feldspar Dust Particles. *J. Phys. Chem. A* **2015**, *119* (11), 2692–2700. https://doi.org/10.1021/jp509839x.

(9)   Fornea, A. P.; Brooks, S. D.; Dooley, J. B.; Saha, A. Heterogeneous Freezing of Ice on Atmospheric Aerosols Containing Ash, Soot, and Soil. *Geophys. Res. Atmos.* **2009**, *114* (D13). https://doi.org/10.1029/2009JD011958.

(10)   Shaw, R. A.; Durant, A. J.; Mi, Y. Heterogeneous Surface Crystallization Observed in Undercooled Water. *J. Phys. Chem. B* **2005**, *109* (20), 9865–9868. https://doi.org/10.1021/jp0506336.

(11)   Hoyle, C. R.; Pinti, V.; Welti, A.; Zobrist, B.; Marcolli, C.; Luo, B.; Höskuldsson, Á.; Mattsson, H. B.; Stetzer, O.; Thorsteinsson, T.; Larsen, G.; Peter, T. Ice Nucleation Properties of Volcanic Ash from Eyjafjallajökull. *Atmos. Chem. Phys.* **2011**, *11* (18), 9911–9926. https://doi.org/10.5194/acp-11-9911-2011.

(12)   Diehl, K.; Matthias-Maser, S.; Jaenike, R.; Mitra, S. K. The Ice Nucleating Ability of Pollen: Part II. Laboratory Studies in Immersion and Contact Freezing Modes. *Atmos. Res.* **2002**, *61* (2), 125–133. https://doi.org/10.1016/S0169-8095(01)00132-6.

(13)   Pummer, B. G.; Bauer, H.; Bernardi, J.; Bleicher, S.; Grothe, H. Suspendable Macromolecules Are Responsible for Ice Nucleation Activity of Birch and Conifer Pollen. *Atmos. Chem. Phys.* **2012**, *12* (5), 2541–2550. https://doi.org/10.5194/acp-12-2541-2012.

(14)   Iannone, R.; Chernoff, D. I.; Pringle, A.; Martin, S. T.; Bertram, A. K. The Ice Nucleation Ability of One of the Most Abundant Types of Fungal Spores Found in the Atmosphere. *Atmos. Chem. Phys.* **2011**, *11* (3), 1191–1201. https://doi.org/10.5194/acp-11-1191-2011.

(15)   Creamean, J. M.; Ceniceros, J. E.; Newman, L.; Pace, A. D.; Hill, T. C. J.; DeMott, P. J.; Rhodes, M. E. Evaluating the Potential for Haloarchaea to Serve as Ice Nucleating Particles. *Biogeosciences* **2021**, *18* (12), 3751–3762. https://doi.org/10.5194/bg-18-3751-2021.

(16)   DeMott, P. J. An Exploratory Study of Ice Nucleation by Soot Aerosols. *J. Appl. Meteorol. Climatol.* **1990**, *29* (10), 1072–1079. https://doi.org/10.1175/1520-0450(1990)029<1072:AESOIN>2.0.CO;2.

(17)   Grawe, S.; Augustin-Bauditz, S.; Clemen, H.-C.; Ebert, M.; Eriksen Hammer, S.; Lubitz, J.; Reicher, N.; Rudich, Y.; Schneider, J.; Staacke, R.; Stratmann, F.; Welti, A.; Wex, H. Coal Fly Ash: Linking Immersion Freezing Behavior and Physicochemical Particle Properties. *Atmos. Chem. Phys.* **2018**, *18* (19), 13903–13923. https://doi.org/10.5194/acp-18-13903-2018.

(18)   Umo, N. S.; Murray, B. J.; Baeza-Romero, M. T.; Jones, J. M.; Lea-Langton, A. R.; Malkin, T. L.; O'Sullivan, D.; Neve, L.; Plane, J. M. C.; Williams, A. Ice Nucleation by Combustion Ash Particles at Conditions Relevant to Mixed-Phase Clouds. *Atmos. Chem. Phys.* **2015**, *15* (9), 5195–5210. https://doi.org/10.5194/acp-15-5195-2015.

(19)   Ganguly, M.; Ariya, P. A. Ice Nucleation of Model Nanoplastics and Microplastics: A Novel Synthetic Protocol and the Influence of Particle Capping at Diverse Atmospheric Environments. *ACS Earth Space Chem.* **2019**, *3* (9), 1729–1739. https://doi.org/10.1021/acsearthspacechem.9b00132.

(20)   Aeschlimann, M.; Li, G.; Kanji, Z. A.; Mitrano, D. M. Potential Impacts of Atmospheric Microplastics and Nanoplastics on Cloud Formation Processes. *Nat. Geosci.* **2022**, *15* (12), 967–975. https://doi.org/10.1038/s41561-022-01051-9.

(21)   Dris, R.; Gasperi, J.; Rocher, V.; Saad, M.; Renault, N.; Tassin, B. Microplastic Contamination in an Urban Area: A Case Study in Greater Paris. *Environ. Chem.* **2015**, *12* (5), 592–599. https://doi.org/10.1071/EN14167.

(22)   O'Brien, S.; Rauert, C.; Ribeiro, F.; Okoffo, E. D.; Burrows, S. D.; O'Brien, J. W.; Wang, X.; Wright, S. L.; Thomas, K. V. There's Something in the Air: A Review of Sources, Prevalence and Behaviour of Microplastics in the Atmosphere. *Sci. Total Environ.* **2023**, *874*, 162193. https://doi.org/10.1016/j.scitotenv.2023.162193.

(23)   Morales, A. C.; Tomlin, J. M.; West, C. P.; Rivera-Adorno, F. A.; Peterson, B. N.; Sharpe, S. A. L.; Noh, Y.; Sendesi, S. M. T.; Boor, B. E.; Howarter, J. A.; Moffet, R. C.; China, S.; O'Callahan, B. T.; El-Khoury, P. Z.; Whelton, A. J.; Laskin, A. Atmospheric Emission of Nanoplastics from Sewer Pipe Repairs. *Nat. Nanotechnol.* **2022**, *17* (11), 1171–1177. https://doi.org/10.1038/s41565-022-01219-9.

(24)   Brahney, J.; Mahowald, N.; Prank, M.; Cornwell, G.; Klimont, Z.; Matsui, H.; Prather, K. A. Constraining the Atmospheric Limb of the Plastic Cycle. *Proc. Natl Acad. Sci. USA* **2021**, *118* (16), e2020719118. https://doi.org/10.1073/pnas.2020719118.

(25)   Dris, R.; Gasperi, J.; Saad, M.; Mirande, C.; Tassin, B. Synthetic Fibers in Atmospheric Fallout: A Source of Microplastics in the Environment? *Mar. Pollut. Bull.* **2016**, *104* (1), 290–293. https://doi.org/10.1016/j.marpolbul.2016.01.006.

(26)   Finnegan, A. M. D.; Süsserott, R.; Gabbott, S. E.; Gouramanis, C. Man-Made Natural and Regenerated Cellulosic Fibres Greatly Outnumber Microplastic Fibres in the Atmosphere. *Environ. Pollut.* **2022**, *310*, 119808. https://doi.org/10.1016/j.envpol.2022.119808.

(27)   Allen, S.; Allen, D.; Phoenix, V. R.; Le Roux, G.; Durántez Jiménez, P.; Simonneau, A.; Binet, S.; Galop, D. Atmospheric Transport and Deposition of Microplastics in a Remote Mountain Catchment. *Nat. Geosci.* **2019**, *12* (5), 339–344. https://doi.org/10.1038/s41561-019-0335-5.

(28)   Bergmann, M.; Mützel, S.; Primpke, S.; Tekman, M. B.; Trachsel, J.; Gerdts, G. White and Wonderful? Microplastics Prevail in Snow from the Alps to the Arctic. *Science Advances* **2019**, *5* (8), 1157. https://doi.org/10.1126/sciadv.aax1157.

(29)   Vali, G. Quantitative Evaluation of Experimental Results an the Heterogeneous Freezing Nucleation of Supercooled Liquids. *J. Atmos. Sci.* **1971**, *28* (3), 402–409. https://doi.org/10.1175/1520-0469(1971)028<0402:QEOERA>2.0.CO;2.

(30)   Whale, T. F.; Murray, B. J.; O'Sullivan, D.; Wilson, T. W.; Umo, N. S.; Baustian, K. J.; Atkinson, J. D.; Workneh, D. A.; Morris, G. J. A Technique for Quantifying Heterogeneous Ice Nucleation in Microlitre Supercooled Water Droplets. *Atmos. Meas. Tech.* **2015**, *8* (6), 2437–2447. https://doi.org/10.5194/amt-8-2437-2015.

(31)   Xi, Y.; Xu, C.; Downey, A.; Stevens, R.; O. Bachelder, J.; King, J.; L. Hayes, P.; K. Bertram, A. Ice Nucleating Properties of Airborne Dust from an Actively Retreating Glacier in Yukon, Canada. *Environ. Sci.* **2022**, *2* (4), 714–726. https://doi.org/10.1039/D1EA00101A.

(32)   Xi, Y.; Mercier, A.; Kuang, C.; Yun, J.; Christy, A.; Melo, L.; T. Maldonado, M.; A. Raymond, J.; K. Bertram, A. Concentrations and Properties of Ice Nucleating Substances in Exudates from Antarctic Sea-Ice Diatoms. *Environ. Sci. Process. Impacts* **2021**, *23* (2), 323–334. https://doi.org/10.1039/D0EM00398K.

(33)   Brunauer, S.; Emmett, P. H.; Teller, E. Adsorption of Gases in Multimolecular Layers. *J. Am. Chem. Soc.* **1938**, *60* (2), 309–319. https://doi.org/10.1021/ja01269a023.

(34)   Osterrieth, J. W. M.; Rampersad, J.; Madden, D.; Rampal, N.; Skoric, L.; Connolly, B.; Allendorf, M. D.; Stavila, V.; Snider, J. L.; Ameloot, R.; Marreiros, J.; Ania, C.; Azevedo, D.; Vilarrasa-Garcia, E.; Santos, B. F.; Bu, X.-H.; Chang, Z.; Bunzen, H.; Champness, N. R.; Griffin, S. L.; Chen, B.; Lin, R.-B.; Coasne, B.; Cohen, S.; Moreton, J. C.; Colón, Y. J.; Chen, L.; Clowes, R.; Coudert, F.-X.; Cui, Y.; Hou, B.; D'Alessandro, D. M.; Doheny, P. W.; Dincă, M.; Sun, C.; Doonan, C.; Huxley, M. T.; Evans, J. D.; Falcaro, P.; Ricco, R.; Farha, O.; Idrees, K. B.; Islamoglu, T.; Feng, P.; Yang, H.; Forgan, R. S.; Bara, D.; Furukawa, S.; Sanchez, E.; Gascon, J.; Telalović, S.; Ghosh, S. K.; Mukherjee, S.; Hill, M. R.; Sadiq, M. M.; Horcajada, P.; Salcedo-Abraira, P.; Kaneko, K.; Kukobat, R.; Kenvin, J.; Keskin, S.; Kitagawa, S.; Otake, K.; Lively, R. P.; DeWitt, S. J. A.; Llewellyn, P.; Lotsch, B. V.; Emmerling, S. T.; Pütz, A. M.; Martí-Gastaldo, C.; Padial, N. M.; García-Martínez, J.; Linares, N.; Maspoch, D.; Suárez del Pino, J. A.; Moghadam, P.; Oktavian, R.; Morris, R. E.; Wheatley, P. S.; Navarro, J.; Petit, C.; Danaci, D.; Rosseinsky, M. J.; Katsoulidis, A. P.; Schröder, M.; Han, X.; Yang, S.; Serre, C.; Mouchaham, G.; Sholl, D. S.; Thyagarajan, R.; Siderius, D.; Snurr, R. Q.; Goncalves, R. B.; Telfer, S.; Lee, S. J.; Ting, V. P.; Rowlandson, J. L.; Uemura, T.; Iiyuka, T.; van der Veen, M. A.; Rega, D.; Van Speybroeck, V.; Rogge, S. M. J.; Lamaire, A.; Walton, K. S.; Bingel, L. W.; Wuttke, S.; Andreo, J.; Yaghi, O.; Zhang, B.; Yavuz, C. T.; Nguyen, T. S.; Zamora, F.; Montoro, C.; Zhou, H.; Kirchon, A.; Fairen-Jimenez, D. How Reproducible Are Surface Areas Calculated from the BET Equation? *Adv. Mater.* **2022**, *34* (27), 2201502. https://doi.org/10.1002/adma.202201502.

(35)   Knopf, D. A.; Anthony, L. M.; Bertram, A. K. Reactive Uptake of O3 by Multicomponent and Multiphase Mixtures Containing Oleic Acid. *J. Phys. Chem. A* **2005**, *109* (25), 5579–5589. https://doi.org/10.1021/jp0512513.

(36)   Seinfeld, J. H.; Pandis, S. N. *Atmospheric Chemistry and Physics: From Air Pollution to Climate Change*, 2nd ed.; John Wiley & Sons: Hoboken, New Jersey, 2006.

(37)   Vig, J. R. UV/Ozone Cleaning of Surfaces. *J. Vac. Sci. Technol. A* **1985**, *3* (3), 1027–1034. https://doi.org/10.1116/1.573115.

(38)   MacManus, L. F.; Walzak, M. J.; McIntyre, N. S. Study of Ultraviolet Light and Ozone Surface Modification of Polypropylene. *J. Polym. Sci., Part A: Polym. Chem.* **1999**, *37* (14), 2489–

2501. https://doi.org/10.1002/(SICI)1099-0518(19990715)37:14<2489::AID-POLA23>3.0.CO;2-G.

(39)   Kang, E.; Root, M. J.; Toohey, D. W.; Brune, W. H. Introducing the Concept of Potential Aerosol Mass (PAM). *Atmos. Chem. Phys.* **2007**, *7* (22), 5727–5744. https://doi.org/10.5194/acp-7-5727-2007.

(40)   Goldstein, H.; Healy, M. J. R. The Graphical Presentation of a Collection of Means. *J. R. Stat. Soc. Ser. A* **1995**, *158* (1), 175. https://doi.org/10.2307/2983411.

(41)   Shardt, N.; N. Isenrich, F.; Waser, B.; Marcolli, C.; A. Kanji, Z.; J. deMello, A.; Lohmann, U. Homogeneous Freezing of Water Droplets for Different Volumes and Cooling Rates. *Phys. Chem. Chem. Phys.* **2022**, *24* (46), 28213–28221. https://doi.org/10.1039/D2CP03896J.

(42)   Hiranuma, N.; Hoffmann, N.; Kiselev, A.; Dreyer, A.; Zhang, K.; Kulkarni, G.; Koop, T.; Möhler, O. Influence of Surface Morphology on the Immersion Mode Ice Nucleation Efficiency of Hematite Particles. *Atmos. Chem. Phys.* **2014**, *14* (5), 2315–2324. https://doi.org/10.5194/acp-14-2315-2014.

(43)   Harrison, A. D.; Lever, K.; Sanchez-Marroquin, A.; Holden, M. A.; Whale, T. F.; Tarn, M. D.; McQuaid, J. B.; Murray, B. J. The Ice-Nucleating Ability of Quartz Immersed in Water and Its Atmospheric Importance Compared to K-Feldspar. *Atmos. Chem. Phys.* **2019**, *19* (17), 11343–11361. https://doi.org/10.5194/acp-19-11343-2019.

(44)   Niemand, M.; Möhler, O.; Vogel, B.; Vogel, H.; Hoose, C.; Connolly, P.; Klein, H.; Bingemer, H.; DeMott, P.; Skrotzki, J.; Leisner, T. A Particle-Surface-Area-Based Parameterization of Immersion Freezing on Desert Dust Particles. *J. Atmos. Sci.* **2012**, *69* (10), 3077–3092. https://doi.org/10.1175/JAS-D-11-0249.1.

(45)   J. Murray, B.; O'Sullivan, D.; D. Atkinson, J.; E. Webb, M. Ice Nucleation by Particles Immersed in Supercooled Cloud Droplets. *Chem. Soc. Rev.* **2012**, *41* (19), 6519–6554. https://doi.org/10.1039/C2CS35200A.

(46)   Hiranuma, N.; Augustin-Bauditz, S.; Bingemer, H.; Budke, C.; Curtius, J.; Danielczok, A.; Diehl, K.; Dreischmeier, K.; Ebert, M.; Frank, F.; Hoffmann, N.; Kandler, K.; Kiselev, A.; Koop, T.; Leisner, T.; Möhler, O.; Nillius, B.; Peckhaus, A.; Rose, D.; Weinbruch, S.; Wex, H.; Boose, Y.; DeMott, P. J.; Hader, J. D.; Hill, T. C. J.; Kanji, Z. A.; Kulkarni, G.; Levin, E. J. T.; McCluskey, C. S.; Murakami, M.; Murray, B. J.; Niedermeier, D.; Petters, M. D.; O'Sullivan, D.; Saito, A.; Schill, G. P.; Tajiri, T.; Tolbert, M. A.; Welti, A.; Whale, T. F.; Wright, T. P.; Yamashita, K. A Comprehensive Laboratory Study on the Immersion Freezing Behavior of Illite NX Particles: A Comparison of 17 Ice Nucleation Measurement Techniques. *Atmos. Chem. Phys.* **2015**, *15* (5), 2489–2518. https://doi.org/10.5194/acp-15-2489-2015.

(47)   Haga, D. I.; Iannone, R.; Wheeler, M. J.; Mason, R.; Polishchuk, E. A.; Fetch Jr., T.; van der Kamp, B. J.; McKendry, I. G.; Bertram, A. K. Ice Nucleation Properties of Rust and Bunt Fungal Spores and Their Transport to High Altitudes, Where They Can Cause Heterogeneous Freezing. *Geophys. Res. Atmos.* **2013**, *118* (13), 7260–7272. https://doi.org/10.1002/jgrd.50556.

(48)   Broadley, S. L.; Murray, B. J.; Herbert, R. J.; Atkinson, J. D.; Dobbie, S.; Malkin, T. L.; Condliffe, E.; Neve, L. Immersion Mode Heterogeneous Ice Nucleation by an Illite Rich Powder Representative of Atmospheric Mineral Dust. *Atmos. Chem. Phys.* **2012**, *12* (1), 287–307. https://doi.org/10.5194/acp-12-287-2012.

(49)   Friedrich, F.; Steudel, A.; Weidler, P. G. Change of the Refractive Index of Illite Particles by Reduction of the Fe Content of the Octahedral Sheet. *Clays Clay Miner.* **2008**, *56* (5), 505–510. https://doi.org/10.1346/CCMN.2008.0560503.

(50)   Vergara-Temprado, J.; Murray, B. J.; Wilson, T. W.; O'Sullivan, D.; Browse, J.; Pringle, K. J.; Ardon-Dryer, K.; Bertram, A. K.; Burrows, S. M.; Ceburnis, D.; DeMott, P. J.; Mason, R. H.; O'Dowd, C. D.; Rinaldi, M.; Carslaw, K. S. Contribution of Feldspar and Marine Organic Aerosols to Global Ice Nucleating Particle Concentrations. *Atmos. Chem. Phys.* **2017**, *17* (5), 3637–3658. https://doi.org/10.5194/acp-17-3637-2017.

(51)   Fröhlich-Nowoisky, J.; Kampf, C. J.; Weber, B.; Huffman, J. A.; Pöhlker, C.; Andreae, M. O.; Lang-Yona, N.; Burrows, S. M.; Gunthe, S. S.; Elbert, W.; Su, H.; Hoor, P.; Thines, E.; Hoffmann, T.; Després, V. R.; Pöschl, U. Bioaerosols in the Earth System: Climate, Health, and Ecosystem Interactions. *Atmos. Res.* **2016**, *182*, 346–376. https://doi.org/10.1016/j.atmosres.2016.07.018.

(52)   González-Pleiter, M.; Edo, C.; Aguilera, Á.; Viúdez-Moreiras, D.; Pulido-Reyes, G.; González-Toril, E.; Osuna, S.; de Diego-Castilla, G.; Leganés, F.; Fernández-Piñas, F.; Rosal, R. Occurrence and Transport of Microplastics Sampled within and above the Planetary Boundary Layer. *Sci. Total Environ.* **2021**, *761*, 143213. https://doi.org/10.1016/j.scitotenv.2020.143213.

(53)   Wang, Y.; Okochi, H.; Tani, Y.; Hayami, H.; Minami, Y.; Katsumi, N.; Takeuchi, M.; Sorimachi, A.; Fujii, Y.; Kajino, M.; Adachi, K.; Ishihara, Y.; Iwamoto, Y.; Niida, Y. Airborne Hydrophilic Microplastics in Cloud Water at High Altitudes and Their Role in Cloud Formation. *Environ. Chem. Lett.* **2023**, *21* (6), 3055–3062. https://doi.org/10.1007/s10311-023-01626-x.

(54)   Malpass, D. M.; Band, E. I. *Introduction to Industrial Polypropylene: Properties, Catalysts, Processes*; Scrivener Publishing LLC, John Wiley & Sons: Salem, Massachusetts; Hoboken, New Jersey, 2012.

(55)   Kanji, Z. A.; Ladino, L. A.; Wex, H.; Boose, Y.; Burkert-Kohn, M.; Cziczo, D. J.; Krämer, M. Overview of Ice Nucleating Particles. *Meteorol. Monogr.* **2017**, *58* (1), 1.1-1.33. https://doi.org/10.1175/AMSMONOGRAPHS-D-16-0006.1.

(56)   Patel, T. Y.; Buttner, M.; Rivas, D.; Cross, C.; Bazylinski, D. A.; Seggev, J. Variation in Airborne Fungal Spore Concentrations among Five Monitoring Locations in a Desert Urban Environment. *Environ. Monit. Assess.* **2018**, *190* (11), 634. https://doi.org/10.1007/s10661-018-7008-5.

(57)   Bogler, S.; Borduas-Dedekind, N. Lignin's Ability to Nucleate Ice via Immersion Freezing and Its Stability towards Physicochemical Treatments and Atmospheric Processing. *Atmos. Chem. Phys.* **2020**, *20* (23), 14509–14522. https://doi.org/10.5194/acp-20-14509-2020.

(58)   Gute, E.; David, R. O.; Kanji, Z. A.; Abbatt, J. P. D. Ice Nucleation Ability of Tree Pollen Altered by Atmospheric Processing. *ACS Earth Space Chem.* **2020**, *4* (12), 2312–2319. https://doi.org/10.1021/acsearthspacechem.0c00218.

(59)   Dymarska, M.; Murray, B. J.; Sun, L.; Eastwood, M. L.; Knopf, D. A.; Bertram, A. K. Deposition Ice Nucleation on Soot at Temperatures Relevant for the Lower Troposphere. *Geophys. Res. Atmos.* **2006**, *111* (D4). https://doi.org/10.1029/2005JD006627.

(60)   Friedman, B.; Kulkarni, G.; Beránek, J.; Zelenyuk, A.; Thornton, J. A.; Cziczo, D. J. Ice Nucleation and Droplet Formation by Bare and Coated Soot Particles. *Geophys. Res. Atmos.* **2011**, *116* (D17). https://doi.org/10.1029/2011JD015999.

(61)   Kanji, Z. A.; Welti, A.; Chou, C.; Stetzer, O.; Lohmann, U. Laboratory Studies of Immersion and Deposition Mode Ice Nucleation of Ozone Aged Mineral Dust Particles. *Atmos. Chem. Phys.* **2013**, *13* (17), 9097–9118. https://doi.org/10.5194/acp-13-9097-2013.

(62)   Kozjek, M.; Vengust, D.; Radošević, T.; Žitko, G.; Koren, S.; Toplak, N.; Jerman, I.; Butala, M.; Podlogar, M.; Viršek, M. K. Dissecting Giant Hailstones: A Glimpse into the Troposphere with Its Diverse Bacterial Communities and Fibrous Microplastics. *Sci. Total Environ.* **2023**, *856*, 158786. https://doi.org/10.1016/j.scitotenv.2022.158786.